J Dent Res 73(1):56-66, January, 1994

Deformation of the Human Mandible During Simulated Tooth Clenching

T.W.P. Korioth* and A.G. Hannam**

*Department of Oral Science, Minnesota Dental Research Center for Biomaterials and Biomechanics, School of Dentistry, University of Minnesota, 16-212 Moos Tower, 515 Delaware Street, SE, Minneapolis, Minnesota 55455; **Department of Oral Biology, Faculty of Dentistry, University of British Columbia, 2199 Wesbrook Mall, Vancouver, BC V6T 1Z3, Canada

Abstract. Localized corpus and dental arch distortions measured directly on human and animal mandibles suggest complex deformation patterns at other mandibular sites during functional loading. To describe these, we simulated selected static bites on a three-dimensional finite element computer model of the human jaw. Five clenching tasks were modeled: intercuspal position, left group function, left group function plus balancing contact, incisal clenching, and right molar clenching. Under conditions of static equilibrium and within the limitations of the current modeling approach, the human jaw deforms elastically during symmetrical and asymmetrical clenching tasks. This deformation is complex, and includes the rotational distortion of the corpora around their axes. In addition, the jaw also deforms parasagittally and transversely. The degree of distortion depended on each clenching task, with actual deformations being relatively small and ranging from 0.46 mm to 1.06 mm for the tasks modeled when all sites were taken into account. The predicted overall narrowing of the dental arch is consistent with clinical reports in the literature during similar, although not identical, static jaw function. The predicted regional deformations of the upper condylar surfaces imply differential loading at their upper surfaces. Although still constrained to forceful static biting conditions, the simulated mandibular and dental arch distortions should be taken into consideration in the design and testing of prosthetic devices in the lower jaw.

Key words. Mandible, Deformation, Finite Element Analysis.

Received April 23, 1993; Accepted October 1, 1993
This investigation was supported by the Medical Research Council of Canada.

Introduction

Several human clinical studies have demonstrated changes in lower posterior dental arch width during function. When various mediolateral arch dimensions were evaluated during dynamic jaw movements such as retraction and protrusion, the lower dental arch has been shown to widen (Burch, 1972; Omar and Wise, 1981) or narrow (Burch, 1972; Goodkind and Heringlake, 1972; Omar and Wise, 1981; Grant, 1986), respectively. A decrease in lower dental arch width has also been measured at open and protruded jaw positions (Jung, 1957, 1959, 1960; McDowell and Regli, 1961; Osborne and Tomlin, 1964; Regli and Kelly, 1967; De Marco and Paine, 1974; Fischman, 1990). In these studies, the tasks involved muscle co-activation at various non-occlusal mandibular positions, and dental occlusion was purposefully neglected to avoid the effect of periodontal and alveolar bone deformation on mandibular distortion. Deformation of the paradental tissues seems to be significant at low force levels (Mühlemann and Zander, 1954).

Few investigations have dealt with the measurement of dental arch deformation during static biting. Clenching between premolar and molar teeth on the working side seems to increase the dental arch width at more posterior tooth locations (Koeck and Sander, 1978), and induce tooth movement on the balancing side (Picton, 1962), both of which are thought to be caused by jaw deformation due to muscle activity. Also, the inclusion of a balancing-side contact during a working-side molar clench apparently narrows the arch between the second molars (Koeck and Sander, 1978).

Animal experiments have shown that the mammalian mandibular corpus can deform transversely, parasagittally, and in a rotational manner during function, and that these patterns may occur alone, in combination, unilaterally, or bilaterally (Kakudo *et al.*, 1973; Weijs and De Jongh, 1977; Hylander, 1979a,b, 1977; Hylander and Bays, 1979; Hylander and

Crompton, 1986; Hylander *et al.*, 1987) (see Fig. 1). In the monkey, jaw deformations have proved to be complex and are characterized mainly by vertical and rotational components. During unilateral biting, the macaque's jaw seems to deform around its long axis on the working side (Hylander, 1979a). This rotational deformation could have a variable transverse effect on the dental arch. It would seem that during unilateral biting the dental arch width could contract posteriorly and at the same time expand anteriorly.

In the present study, we used a model of the human jaw to describe the three-dimensional (3D) deformation of the lower jaw border during simulated clenching tasks. We tested the hypothesis that rotational deformation occurs in the human mandible during function, and we compared the transverse deformation of the dental arch with that of the lower border.

Materials and methods

A freshly dissected and fully dentate human mandible was immersed in saline and imaged in the frontal and mid-sagittal planes by computerized tomography (CT) (Siemens Somatom DR 2, Siemens GmbH, München, Germany). The images were obtained with thin collimation (1-mm thickness) at small slice intervals (2-mm increments). All dental and cortical bone outlines were traced sequentially on acetate overlays, digitized, and assembled into a three-dimensional (3-D) wireframe model by means of commercially available software (I-DEAS® 6.0, SDRC, Milford, OH). Each mandibular outline was divided into several cubic splines at specific landmarks to allow for better control of the geometry and to minimize the distortion of the finite element (FE) mesh, thus increasing the predictive accuracy of the model. The interconnection of the lower landmarks formed a spline which ran lingually from the mid-region of the corpus along the mylohyoid ridge up to the condylar neck and then back along the lateral region of the human corpus to its anterior midline. The upper landmarks formed a spline which outlined the superior and lateral-most portion of the alveolar bone, followed by the coronoid process and notch, and the upper surface of the condyle. Teeth were modeled with single or bifurcated roots, including their periodontal ligaments and laminae durae (see Fig. 2C). The structure of the temporomandibular joints was modeled as a two-layered "cap", where the first cap consisted of the combined thicknesses of condylar, articular, and temporal fibrocartilage, and the second of temporal cortical bone (Hansson *et al.*, 1977). This permitted analysis of the stress distribution on the condyles, while allowing for the "buffering" effect of the articular disk against the rigid temporal bone. In the wireframe model, each group of three or four interconnected curves formed a closed boundary area (*i.e.*, mesh area), and five or six interrelated areas formed wedge or brick-shaped volumes (*i.e.*, mesh volumes). The final model consisted of 5926 elements with 7375 nodes (see Fig. 2A). The elements were either linear wedge or linear brick solids with 6 or 8 nodes, respectively.

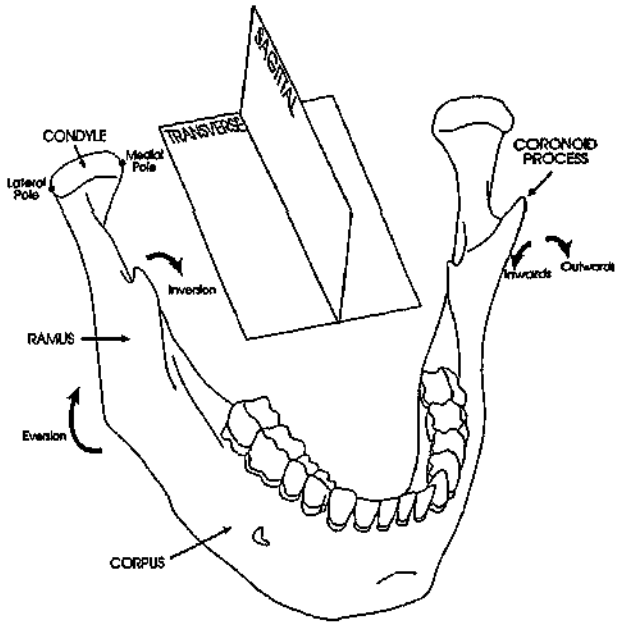

Figure 1. Diagram illustrating the relevant nomenclature used to explain mandibular deformation. In addition to the possible parasagittal and transverse deformation patterns, the corpus and ramus on each side may undergo rotations such as the one in which the lower mandibular border is everted and the coronoid process is deformed inward (*i.e.*, inverted).

Thus, the solution was performed as a linearly elastic simulation.

The different structures in the FE model of the human jaw were assigned material characteristics conforming to data available in the literature. Cortical bone was considered to behave orthotropically, that is, its properties were assumed to be dissimilar in three perpendicular directions, with the largest elastic constants oriented along the longitudinal axis of the jaw (Arendts and Sigolotto, 1989, 1990; Dechow *et al.*, 1992, 1993). Since the elastic properties of human mandibular cancellous bone are unknown, isotropic values determined from human tibial bone material were used (Ashman *et al.*, 1987). The orthotropic material properties for cortical bone were assigned by use of a local coordinate system corresponding to natural mandibular geometry, with a curve representing the long axis of the jaw. This curve ran along the entire lower jaw border, and its longitudinal direction represented the material x-axis of each bone element. The y-axis was aligned perpendicular to the x-axis but tangentially to each related jaw cross-section. The material z-axis was derived from the x and y axes and lay perpendicular to both. The elastic properties of the periodontal ligament are thought to vary with root length, at least for human premolar teeth (Mandel *et al.*, 1986). In the model, therefore, the periodontal space of each tooth was divided into apical, middle, and coronal thirds, and each third was assigned a different elastic stiffness. These parameters did not differ among teeth. Since the majority of studies dealing with me-

Table 1. Isotropic material properties assigned to the FE model of the human jaw

	Isotropic Materials (parallel to long tooth axis)		
	E (in GPa)	ν	Allowable Tensile Stress (GPa)
Enamel[1]	80.0	0.30	
Dentin[2]	17.6	0.25	
Fibrocartilage[3]	0.006	0.47	
Periodontium[4,5,6]			
Upper root third	0.0032	0.45	0.0024
Middle root third	0.0027	0.45	0.0024
Basal root third	0.0025	0.45	0.0024
Cancellous Bone[7]	0.378	0.30	

E Young's Modulus of Elasticity.

ν Poisson's Ratio.

GPa GigaPascal (1 GPa = 10^9 Pa = 10^9 N/m^2).

References: [1]Craig *et al.*, 1961; [2]Craig and Peyton, 1958; [3]Wong and Carter, 1988; [4]Mandel *et al.*, 1986; [5]Widera *et al.*, 1976; [6]Ralph, 1982; [7]Ashman *et al.*, 1987.

chanical properties of the periodontal ligament have measured its tensile strength characteristics, the model was also given maximum tensile stress parameters (*i.e.*, yield points) along the dental long axes (Ralph, 1982). All remaining tissues were assumed to be isotropic (*i.e.*, directionally independent). Although enamel and dentin also have anisotropic material characteristics (Howard *et al.*, 1990) and possess regional stiffness variations (Craig *et al.*, 1961), they were modeled isotropically due to the difficulty of establishing principal axes of anisotropy (Lees and Rollins, Jr., 1972). The isotropic (Craig and Peyton, 1958; Widera *et al.*, 1976; Wong and Carter, 1988) and orthotropic material properties assigned to all structural elements of the model are listed in Tables 1 and 2, respectively.

The FE model was submitted to validation tests which have been published elsewhere (Korioth, 1992). The predicted principal strains during complex corpus bending were compared with strain readings measured experimentally from six rosettes placed on the periosteal cortical surface of the freshly excised mandible, near the left lower corpus border in the molar region. According to experiments performed on living animals, the mammalian jaw is subjected to multiple forces which generate complex bending patterns during masticatory function. For example, during the power stroke of mastication in macaques, the mandibular corpora undergo parasagittal and transverse bending, and torsion (Hylander 1979). Since these complex patterns are difficult to imitate, the mandible was subjected to controlled artificial loads that could be more accurately defined. Corporal torsion in the jaw was induced by the application of artificial loads in a medial direction to the left gonial region. The mandible was restrained from movement by embedding both the condyles and the anterior dentition, including the premolars, in acrylic resin, which was rigidly attached to a metal framework. Validation of the model revealed small differences between observed and predicted principal strains (from 1.0% to 9.2%), demonstrating the model's potential to predict physical events on the periosteal cortical surface of the jaw. These small inconsistencies were probably due to the model's inner structural inaccuracies and the incomplete and limited assignment of rheological properties to its various components.

To analyze further the interdependency between the material properties and the geometry of cortical bone upon principal strains in the corpus region, multiple sensitivity analyses were performed on the model during the simulated medial loading of the jaw at the left gonial angle (Korioth, 1992). These simulations indicated that the material properties which affected predicted cortical principal strain the most were the orthotropic shear moduli (alone or in combination—up to 30% in difference from the unchanged, original state), the orientation of material properties of the elements (37%), and the absence of cancellous bone (up to 34%). Alterations to the geometry of the molar cross-section, such as increases in the external corpus dimensions, had the greatest effect on principal strain magnitudes (up to 16%). Modifications to geometric variables affected the principal strain values only locally, in the vicinity of the translated nodes.

The model was then used to simulate five static biting tasks. These tasks involved clenching in the intercuspal position (ICP); with the teeth in left group function (LGF) and in left group function with a cross-arch balancing contact on the second molar (LGF+B); incisal clenching (INC); and right unilateral molar clenching (RMOL). In ICP, the canines, premolars, and molars were bilaterally and vertically restrained from movement (excluding the right third molar, which was partially erupted). In LGF, the left canines, premolars, and molars were vertically restrained; in addition to these teeth, the right

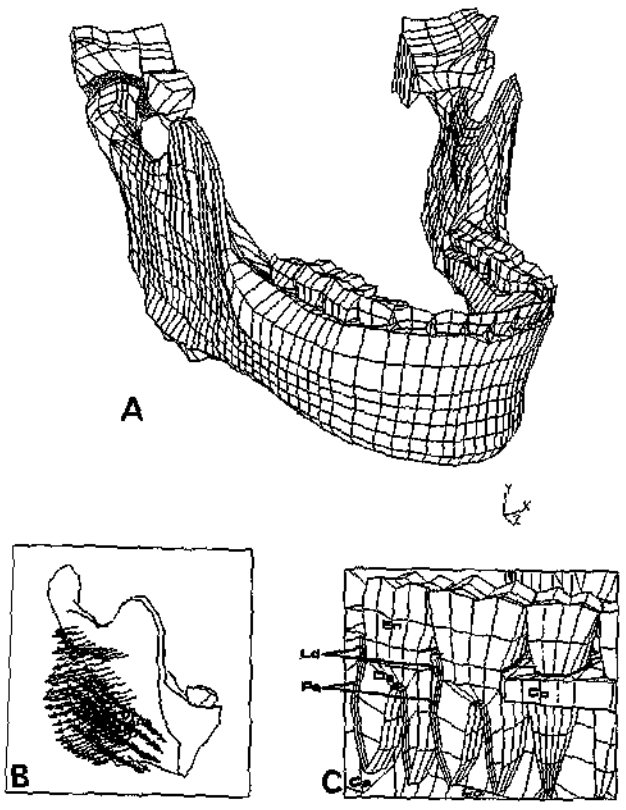

Figure 2. FE model of the dentate human mandible. (A) is a hidden line view of the discretized element mesh seen antero-laterally from the right side. Dental and articular restraints, as well as the muscle loads, have been omitted for clarity. Some elements of the right temporomandibular joint have been deleted to show the presence of a fibrocartilagenous pad (stippled) between the condyle and the temporal bone. (B) shows the right ramus with multiple parallel vectors simulating the masseter muscle loads. All vectors are graphically represented by their x, y, and z components and appear to be embedded in the model due to the nature of the display. In (C), a cut window of the right corpus displays the underlying tissue components. Many cancellous bone elements were deleted to reveal the dental roots. Abbreviations: Co, cortical bone; Ca, cancellous bone; En, enamel; De, dentin; Ld, lamina dura; Pe, periodontal ligament.

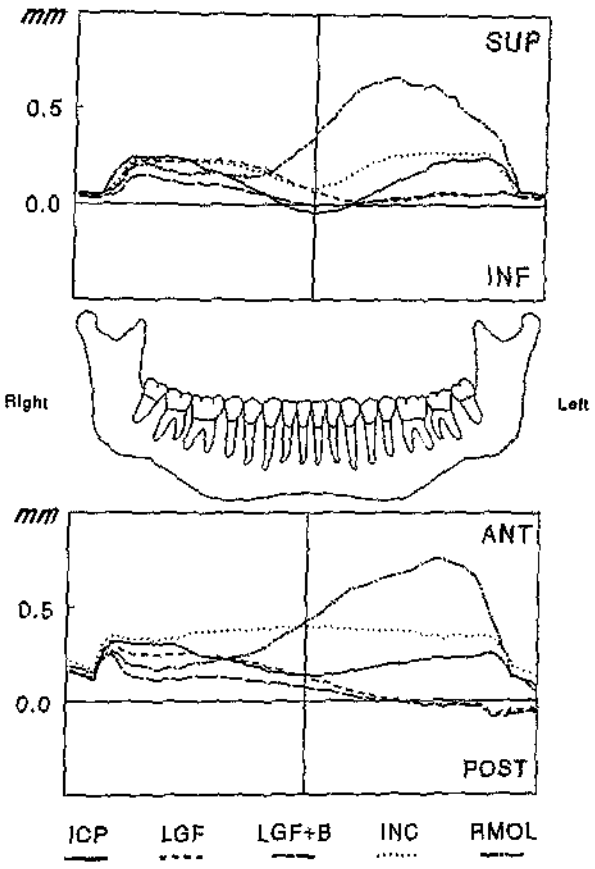

Figure 3. Supero-inferior (upper graph) and antero-posterior (lower graph) deformations of the lower jaw border for the 5 simulated clenching tasks. In each case, the horizontal axis represents the positions of nodes along the lower border of the mandible from right to left condyle. The vertical axis represents displacements in mm.

second molar was restrained in LGF+B. During INC and RMOL, the four incisors and the first right molar, respectively, were not allowed to translate upward.

To simulate muscle forces over wide areas of attachment, the model was loaded with multiple force vectors. Groups of parallel vectors simulated nine pairs of masticatory muscles (superficial and deep masseter; anterior, middle, and posterior temporalis; medial pterygoid; superior and inferior lateral pterygoid; and anterior digastric) assumed to be directly attached to bone (see Fig. 2B). Their directions were derived algebraically as unit vectors (*i.e.*, direction cosines) from single vectors of muscular attachment available in the literature and summarized in Table 3. The magnitude of the total muscle force (M_n) exerted by each muscle during isometric contraction was given by the product

$$[X_{M_i} \cdot K] \cdot EMG_{M_i} = M_n$$

where X_{M_i} is the cross-sectional area of muscle M_i in cm^2, K is a general conversion constant for skeletal muscle (expressed in N/cm^2), and EMG_{M_i} is the ratio or scaled value of the muscle contraction relative to its maximum possible activity for any task (Pruim *et al.*, 1980; Weijs and Hillen, 1984). The product $[X_{M_i} \cdot K]$ is referred to as the Weighting Factor given to the muscle M_i, and the value EMG_{M_i} as its Scaling Factor (Table 4). The product of M_n and its corresponding unit vector thus yielded the orthogonal vector force components, which were subsequently proportioned between the nodes comprising the corresponding area of muscle attachment (see Table 4). In the case of nodes which included parts of two muscles, their respective force components were vectorially combined (Korioth *et al.*, 1992).

For occlusal tasks involving posterior teeth, the model was restrained from movement at the buccal and central thirds of the occlusal surfaces. For those involving the anterior teeth, restraints were placed on the entire incisal surface

Table 2. Orthotropic material properties assigned to the cortical bone in the FE model of the human jaw

	Orthotropic Materials								
	E (in GPa)			ν			G (in GPa)		
	X	Y	Z	XY	YZ	XZ	XY	YZ	XZ
Cortical Bone									
Symphyseal[9]	22.9	14.2	10.5	0.19	0.31	0.29	6.0	3.7	4.8
Canine-PM[9]	25.5	14.5	10.2	0.15	0.30	0.25	6.2	3.4	5.0
First Molar[9]	19.5	13.6	10.2	0.39	0.20	0.55	6.2	4.1	5.9
M2-M3[9]	19.7	14.0	10.9	0.37	0.25	0.47	6.2	4.2	5.0
Ramus[10,11]	17.0	6.9	8.2	0.31	0.33	0.31	4.6	2.9	2.8

E Young's Modulus of Elasticity.
ν Poisson's Ratio.
G Shear Modulus.
GPa GigaPascal (1 GPa = 10^9 Pa=10^9 N/m^2).
X AXIAL (long axis of the mandible); Y, TANGENTIAL (perpendicular to X and tangential to cortical cross-section); Z, RADIAL (perpendicular to XY plane).
PM Premolar; M2, Second Molar; M3, Third Molar.
References: [9]Dechow *et al.*, 1992, 1993; [10]Arendts and Sigolotto, 1989; [11]Arendts and Sigolotto, 1990.

Table 3. Directions of muscular orthogonal components derived as unit vectors (i.e., direction cosines) from single vectors of muscular attachment

	Right Side			Left Side		
	cos-x	cos-y	cos-z	cos-x	cos-y	cos-z
Superficial Masseter	-0.207	0.884	0.419	0.207	0.884	0.419
Deep Masseter	-0.546	0.758	-0.358	0.546	0.758	-0.358
Medial Pterygoid	0.486	0.791	0.373	-0.486	0.791	0.373
Anterior Temporalis	-0.149	0.988	0.044	0.149	0.988	0.044
Middle Temporalis	-0.222	0.837	-0.500	0.222	0.837	-0.500
Posterior Temporalis	-0.208	0.474	-0.855	0.208	0.474	-0.855
Inferior Lateral Pterygoid	0.630	-0.174	0.757	-0.630	-0.174	0.757
Superior Lateral Pterygoid	0.761	0.074	0.645	-0.761	0.074	0.645
Anterior Digastric	-0.244	-0.237	-0.940	0.244	-0.237	-0.940

When seen from the front, the x-z plane was parallel to the floor, with the +x axis oriented toward the right, the +y axis running upward, and the +z axis oriented forward (anteriorly).

of each tooth involved. These restraints acted perpendicularly to the occlusal plane (y-direction) at the lower supporting cusps, allowing freedom of displacement in the horizontal plane. Restraints were also placed bilaterally at the endosteal cortical surfaces of the temporal bones. These limited movement in three dimensions and simulated fixation of the system at the cranium. The five clenches were simulated with both condyles centered in their glenoid fossae. All simulations were carried out with the I-DEAS® package on a Hewlett-Packard 9000-series-380 UNIX®-based minicomputer with a high-resolution workstation (HP 98789A) and peripherals.

Results

The model of the mandible deformed differently for each clenching task. When all mandibular sites were taken into account, actual deformation values were relatively small. Fig. 3 shows the supero-inferior and the antero-posterior deformations of the lower jaw border. In both graphs, the horizontal axis represents the lower border from the right to the left condyle, and the vertical axis the amount of deformation. The upper graph shows that the lower corpus deformed upward during all clenching tasks. The lower graph shows that the lower jaw border also deformed forward. The most significant

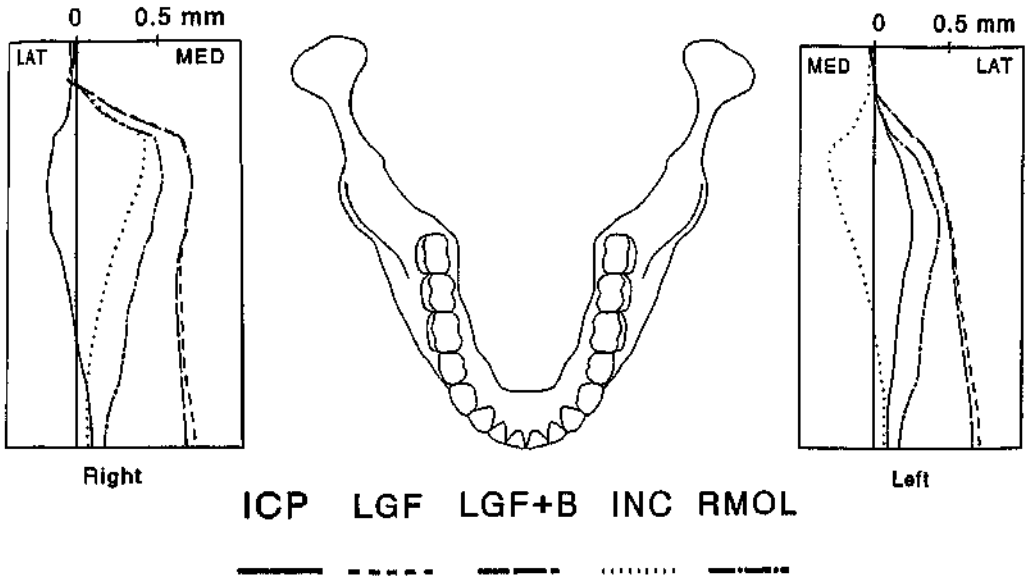

Figure 4. Transverse deformation of the lower jaw border for the 5 simulated clenching tasks. In each case, the horizontal axis represents the medial (MED) and lateral (LAT) deformations, and the vertical axis represents the positions of nodes from condyle to menton.

deformations occurred on the balancing side when clenching was carried out on the right first molar. The large deformation on the balancing side was probably due to the absence of contacts on this side.

Fig. 4 shows the transverse deformations of the lower jaw border. During ICP, the lower border deformed outward, due mainly to the high activity of the masseter muscle. However, the lower border deformed inward during INC, probably due to a strong activity of the medial and inferior lateral pterygoid muscles. In both eccentric lateral positions LGF and LGF+B, the jaw greatly deformed toward the left; this was probably due to a relatively high activity of the right medial pterygoid muscle pulling the jaw medially.

The combination of transverse deformations measured at five locations at the dental arch and the lower jaw border is shown in Fig. 5. The sketch at the top illustrates these locations. Changes in dental arch width were measured at five pairs of teeth from molar to canines, and changes in jaw width were measured at five pairs of homologous, projected locations on the lower jaw border. During ICP, the unfilled bars to the right indicated an overall transverse expansion of the lower jaw border. This expansion was larger posteriorly than anteriorly. Here, the dental arch expanded only between the second molars, and contracted unevenly at more anterior tooth locations. During LGF and LGF+B, the dental arch contracted but the lower jaw border expanded at more anterior sites. During INC, the dental arch contracted the most, and the lower jaw border expanded at more anterior sites. During RMOL, the posterior dental arch contraction was accompanied by an expansion of the lower jaw border posteriorly.

Figs. 6 to 10 show frontal and horizontal views of the model's undeformed and deformed states during the five clenching tasks. In each Fig., the undeformed state depicts the model with its structural elements in their unloaded condition; the deformed state represents one in which the action of the muscle loads and counteractions at the bite point and cranium have displaced the structural elements, and in which the model has reached a state of static equilibrium. In order to make the mandibular deformation more apparent in those Fig., the maximum displacement was magnified to equal 10% of the display screen width, and all remaining smaller deformations were scaled to this maximum value.

The expansion of the lower jaw border during ICP and its contraction during INC were accompanied by the inward rotation of both coronoid processes during ICP and their outward rotation during INC. These results indicated a strong rotation of the rami during symmetrical clenching tasks. Whereas the lateral condylar poles deformed upward during ICP, the medial poles did so during INC, suggesting differential surface loading at the condyles for these two tasks.

During asymmetrical clenching, such as LGF, LGF+B, and RMOL, the balancing-side corpus deformed strongly outward and upward. These patterns, coupled with an overall anterior jaw deformation, indicated a corkscrew-like or helical deformation of the mandible toward the working side. At the condylar level, the lateral condylar pole on the balancing side seemed to be most distorted, deforming upward and forward.

Discussion

The model's predictions confirm that rotational deformations occur in the human mandible. Rotational distortion originates at the rami due to the action of the masticatory muscles and is manifested in the dental arch and at the condyles. The mammalian jaw thus deforms elastically during static function, and the magnitude of the predicted stresses seems to be within the elastic range of the materials studied, in particular the cortical bone of the corpus.

The general upward deformation of the lower jaw border during all clenching tasks supports the notion of parasagittal bending of the corpus. However, the bilateral superior deformation seems to contradict the results from one study performed in humans, where localized mandibular distortion

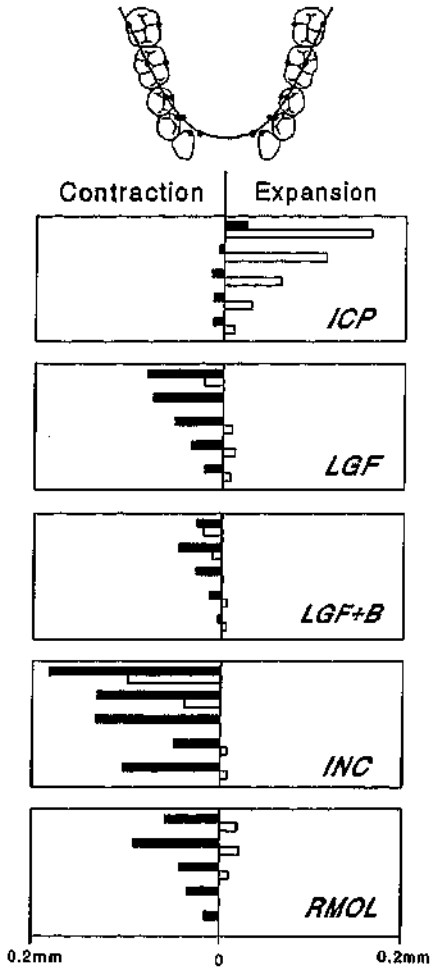

Figure 5. Combination of transverse deformation measured at 5 locations on the dental arch (filled circles) and 5 homologous locations projected vertically to the lower jaw border, shown here as a continuous line. Changes in dental arch and jaw border widths during the 5 deformed states are illustrated by filled and unfilled bars, respectively.

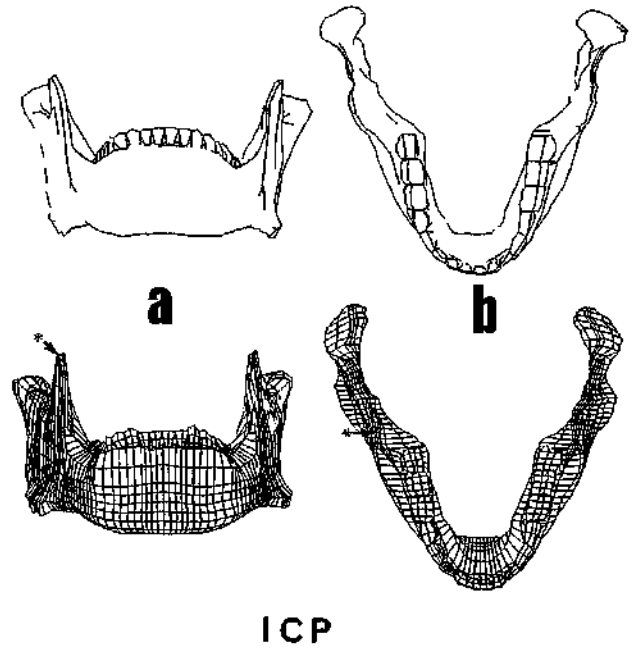

Figure 6. Mandibular deformation during a simulated intercuspal clench (ICP). Frontal (a) and horizontal (b) hidden line views of the FE model in its undeformed (upper) and deformed (lower) states. In this and all subsequent Figs., only the outline of the model is shown in its undeformed state. In addition, the restraints, loads, and articular elements have been omitted. The maximum jaw deformation was 0.46 mm and occurred at the right coronoid process (shown by an asterisk). The maximum deformation was magnified 35 times to equal 10% of the display screen.

was measured *in vivo* with inductance strain gauges on screws rigidly attached to the gonial and symphyseal regions (Marx, 1966). This study showed that during a unilateral molar clench, the working-side corpus deformed downward and the balancing-side corpus upward. Although our model seemed to deform upward on both sides, the results shown in the upper graph on Fig. 3 indicated a slight convex (oriented downward) deformation on the working side and an evident concave deformation on the balancing side. In this graph, the position of the x-axis could have shifted superiorly if the vertical restraints imposed on the dental surfaces would have allowed freedom of movement of the jaw in the inferior direction. Since technical limitation impeded this freedom in our simulations, the results actually confirm Marx's results (1966) but allow only for qualitative comparisons between these experiments.

The anterior deformation of the lateral condylar poles, predicted by the model for the majority of clenching tasks, supports similar suggestions made by others (Hüls *et al.*, 1985). Hüls *et al.* (1985) speculated that the lateral pterygoid muscle would tense its lateralmost fibers the most during eccentric jaw positions, thus imposing a rotational and anterior deformation on the condyle. In our model, the attachment site of this muscle was restrained to the fovea pterygoidea and did not cover the entire medio-lateral length of the condyle, as in the study by Hüls *et al.* (1985). Hence, the anterior deformation of the lateral condylar pole predicted by our model was probably due to the strong anterior rotational deformation of the ramus, and not the lateral pterygoid muscle *per se*.

The unilateral medial transverse deformation of the balancing-side corpus observed during the left group function tasks (LGF and LGF+B) seems at first glance to be the pattern opposite that observed during the power stroke of mastication in macaques. In the macaque study, the pattern of cortical deformation was measured while the mandible apparently moved through the power stroke toward the balancing side (Hylander *et al.*, 1987). Here, the jaw was being displaced medially at the working side and laterally at the balancing side. In the simulated group function of the model, isometric muscle contraction deformed the mandible laterally at the working side and medially at the balancing side. The simulated task

Table 4. Node number, weighting, and scaling factors assigned to the masticatory muscles for five clenching tasks

	Node Number		Weighting Factor (Newton)	Scaling Factor									
				ICP		LGF		LGF+B		INC		RMOL	
	Right	Left		Right	Left	Right	Left	Right	Left	Right	Left	Right	Left
Superficial Masseter	67	67	190.4	1.00	1.00	0.27	0.18	0.26	0.12	0.40	0.40	0.72	0.60
Deep Masseter	38	38	81.6	1.00	1.00	0.26	0.36	0.26	0.36	0.26	0.26	0.72	0.60
Medial Pterygoid	51	50	174.8	0.76	0.76	0.76	0.07	0.73	0.09	0.78	0.78	0.84	0.60
Anterior Temporalis	43	40	158.0	0.98	0.98	0.07	0.66	0.23	0.54	0.08	0.08	0.73	0.58
Middle Temporalis	18	18	95.6	0.96	0.96	0.06	0.64	0.12	0.57	0.06	0.06	0.66	0.67
Posterior Temporalis	15	15	75.6	0.94	0.94	0.06	0.62	0.08	0.59	0.04	0.04	0.59	0.39
Inferior Lateral Pterygoid	5	5	66.9	0.27	0.27	0.14	0.59			0.71	0.71	0.30	0.65
Superior Lateral Pterygoid	4	4	28.7	0.59	0.59	0.08	0.20			0.50	0.50		
Anterior Digastric	8	8	40.0	0.28	0.28	0.38	0.51	.		0.50	0.50		

ICP - Intercuspal Position; LGF - Left Group Function; LGF+B - Left Group Function plus Balancing Molar Contact; INC - Incisal Clench; RMOL - Right Unilateral Molar Clench.

actually reversed the direction of muscular effort used in chewing. If in fact the distortion patterns described in the macaque mandible during chewing are comparable with those of the human condition, our results highlight the essential differences between jaw deformations described during "normal" dynamic chewing and those observed during static occlusal clenching.

In the horizontal plane, the magnitudes of dental arch contraction simulated in the model fell within the range of dimensions measured in young adults (Burch, 1972). Considered antero-posteriorly at the measured sites, the simulated arch contractions would produce non-uniform curves with peaks at sites of single, restrained teeth, such as RMOL and the balancing-side molar during LGF+B. Several factors could

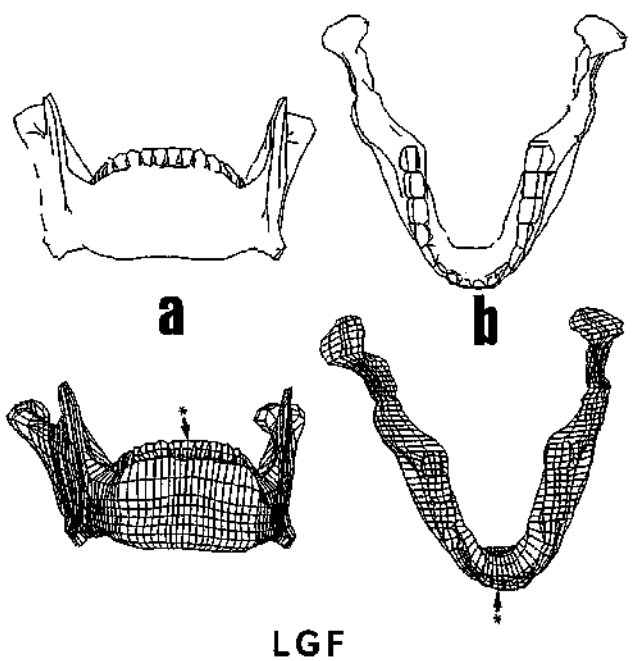

Figure 7. Mandibular deformation during a simulated left group function clench (LGF). Frontal (a) and horizontal (b) hidden line views of the FE model in its upper undeformed and lower deformed states. The maximum jaw deformation was 0.92 mm and occurred at the right central incisor (shown by an asterisk). The maximum deformation was magnified 18 times to equal 10% of the display screen.

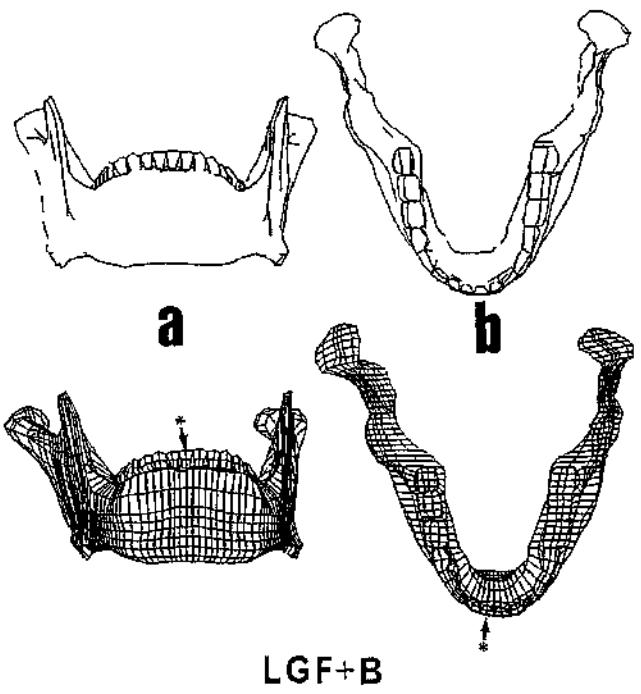

Figure 8. Mandibular deformation during a simulated left group function clench with balancing-side molar contact (LGF+B). Frontal (a) and horizontal (b) hidden line views of the FE model in its upper undeformed and lower deformed states. The maximum jaw deformation was 0.73 mm and occurred at the right central incisor (shown by an asterisk). The maximum deformation was magnified 22 times to equal 10% of the display screen.

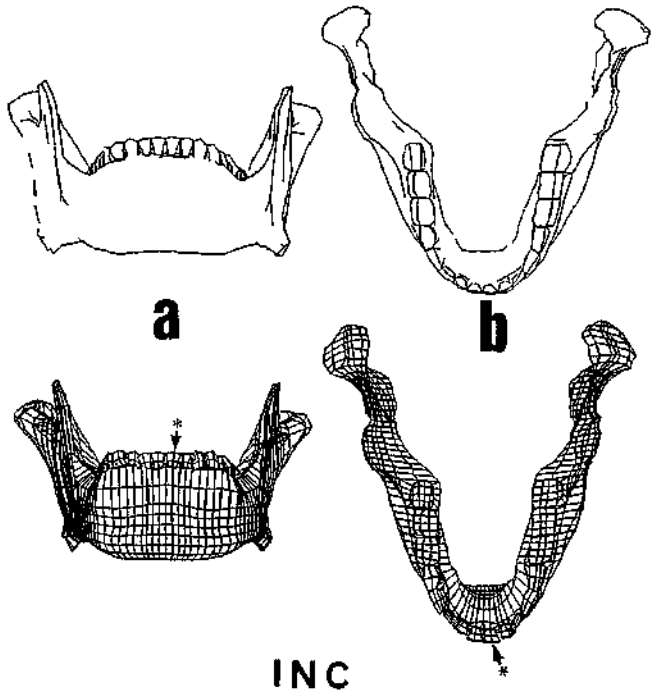

Figure 9. Mandibular deformation during a simulated incisal clench (INC). Frontal (a) and horizontal (b) hidden line views of the FE model in its upper undeformed and lower deformed states. The maximum jaw deformation was 0.62 mm and occurred at the left central incisor (shown by an asterisk). The maximum deformation was magnified 26 times to equal 10% of the display screen.

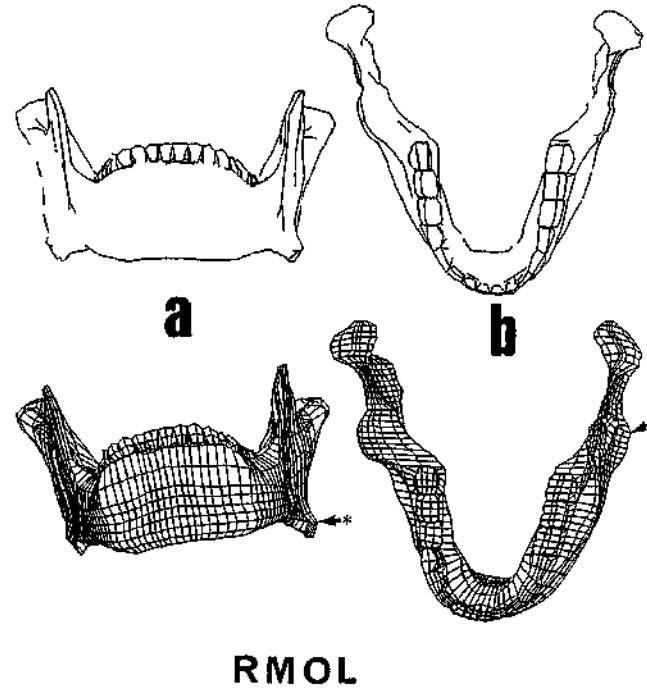

Figure 10. Mandibular deformation during a simulated unilateral right molar clench (RMOL). Frontal (a) and horizontal (b) hidden line views of the FE model in its upper undeformed and lower deformed states. The maximum jaw deformation was 1.06 mm and occurred at the left gonial angle (shown by an asterisk). The maximum deformation was magnified 15 times to equal 10% of the display screen.

have affected these results. First, the dimensions and locations of the dental tissues in the mandible were imprecisely modeled due to the inability of modern CT imaging to depict the paradental tissues adequately, and to the manipulation of outlines to form the element mesh. Second, the material properties of the paradental tissues were necessarily simplified, and the interproximal dental friction was discounted. In the former, the anisotropic and non-linear behavior of the periodontal ligament simply could not be modeled, due to the lack of experimental data. In the latter, interproximal friction coefficients—which have been measured and are available in the dental literature (Osborn, 1961; Southard *et al.*, 1990)—were not included in the modeling process, due to the inability of the software to cope with the complexity of the calculations. This difficulty needs to be overcome in the future by application of other non-linear solvers to the model, since the absence of interproximal contacts could significantly and incorrectly maximize the dental arch deformations during function.

When measuring the mediolateral distances between the lower second molars at several different crown levels or heights in the frontal plane, Jung (1960) determined a gradient of transverse arch contraction, with more arch narrowing at the superior than at more inferior levels of the molar teeth. Although his experiments included only non-occlusal jaw function, Jung concluded that the mandibular corpora had to rotate around their long axes, moving the teeth medially during jaw opening and protrusion. In various studies which evaluated mediolateral dental arch dimensions in humans (Jung, 1957, 1959, 1960; McDowell and Regli, 1961; Osborne and Tomlin, 1964; Regli and Kelly, 1967; De Marco and Paine, 1974; Fischman, 1990), the horizontal jaw deflections measured at the posterior tooth level ranged from 0.03 to 0.78 mm, being consistently higher for protrusive efforts than for jaw opening. The large range of results in the various investigations is probably attributable to differences in methodology, and to variations in muscle activity among the subjects tested. Nevertheless, the notion of rotational deformation of the corpus in humans is substantiated by the predictions of our model, and seems also to apply to functional jaw activities involving dental contacts. This rotational deformation may have a significant effect on prosthetic devices placed on the lower arch, especially if these devices are implants interconnected by rigid superstructures. Cyclic rotational deformation of the corpora could impose complex bending on these structures, with resulting adverse effects on its elements.

Acknowledgments

We gratefully acknowledge the help of Joy D. Scott in all computational aspects of this project. We also thank Dr. Paul C. Dechow for the generous supply of the dissected human jaw,

as well as Dr. Ron L. Sakaguchi and an anonymous reviewer for helpful comments on an earlier version of this manuscript.

References

Arendts FJ, Sigolotto C (1989). Standardabmessungen, Elastizitätskennwerte und Festigkeitsverhalten des Human-Unterkiefers, ein Beitrag zur Darstellung der Biomechanik der Unterkiefer—Teil I. *Biomed Technik* 34:248-255.

Arendts FJ, Sigolotto C (1990). Mechanische Kennwerte des Human-Unterkiefers und Untersuchung zum "in vivo" Verhalten des kompakten Knochengewebes, ein Beitrag zur Darstellung der Biomechanik des Unterkiefers—Teil II. *Biomed Technik* 35:123-130.

Ashman RB, Corin JD, Turner CH (1987). Elastic properties of cancellous bone: Measurement by an ultrasonic technique. *J Biomechan* 20:979-986.

Burch JG (1972). Patterns of change in human mandibular arch width during jaw excursions. *Arch Oral Biol* 17:623-631.

Craig RG, Peyton FA, Johnson DW (1961). Compressive properties of enamel, dental cements and gold. *J Dent Res* 40:936-945.

Craig SC, Peyton FA (1958). Elastic and mechanical properties of human dentin. *J Dent Res* 37:710-718.

DeMarco T, Paine S (1974). Mandibular dimensional change. *J Prosthet Dent* 31:482-485.

Dechow PC, Schwartz-Dabney CL, Ashman RB (1992). Elastic properties of the human mandibular corpus. In: Bone biodynamics in orthodontic and orthopaedic treatment. Vol. 27. Goldstein SA, Carlson DS, editors. Ann Arbor, MI: Craniofacial Growth Series, Center for Human Growth and Development, pp. 299-314.

Dechow PC, Nail GA, Schwartz-Dabney CL, Ashman RB (1993). Elastic properties of human supraorbital and mandibular bone. *Am J Phys Anthropol* 90:291-306.

Fischman B (1990). The rotational aspect of mandibular flexure. *J Prosthet Dent* 64:483-485.

Goodkind RJ, Heringlake CB (1972). Mandibular flexure in opening and closing movements. *J Prosthet Dent* 30:134-138.

Grant AA (1986). Some aspects of mandibular movement: Acceleration and horizontal distortion. *Ann Acad Med (Singapore)* 15:305-310.

Hansson T, Öberg T, Carlsson GE, Kopp S (1977). Thickness of the soft tissue layers and the articular disk of the temporomandibular joint. *Acta Odontol Scand* 35:77-83.

Howard IC, van Noort R, Cardew GE, Noroozi ST (1990). The influence of enamel anisotropy on the stress distribution in teeth (abstract). *J Dent Res* 69(Spec Iss):965.

Hüls A, Walter E, Schulte W, Freesmeyer WB (1985). Computertomographische Stadieneinteilung des dysfunktionellen Gelenkkopfumbaus. *Dtsch Zahnärztl Z* 40:37-51.

Hylander WL (1977). *In vivo* bone strain in the mandible of *Galago crassicaudatus*. *Am J Phys Anthropol* 46:309-326.

Hylander WL (1979a). The functional significance of primate mandibular form. *J Morphol* 160:223-240.

Hylander WL (1979b). Mandibular function in *Galago crassicaudatus* and *Macaca fascicularis*: An *in vivo* approach to stress analysis of the mandible. *J Morphol* 159:253-296.

Hylander WL, Bays R (1979). An *in vivo* strain-gauge analysis of the squamosal-dentary joint reaction force during mastication and incisal biting in *Macaca mulatta* and *Macaca fascicularis*. *Arch Oral Biol* 24:689-697.

Hylander WL, Crompton AW (1986). Jaw movements and patterns of mandibular bone strain during mastication in the monkey *Macaca fascicularis*. *Arch Oral Biol* 31:841-848.

Hylander WL, Johnson KR, Crompton AW (1987). Loading patterns and jaw movements during mastication in *Macaca fascicularis*: a bone-strain, electromyographic, and cineradiographic analysis. *Am J Phys Anthropol* 72:287-314.

Jung F (1957). Über die Reaktionen des Gebisses auf Gaumenplatten. *Dtsch Zahnärztl Z* 12:688-695.

Jung F (1959). Veränderungen des Prothesenlagers unter der Teilprothese. *Dtsch Zahnärztl Z* 14:105-107.

Jung F (1960). Die funktionell-elastische deformation des Kieferknochens und die Eigenbeweglichkeit der Zähne. *Schweiz Mschr Zahnheilk* 70:17-30.

Kakudo Y, Ishida A, Yoshimoto S (1973). Strains in dog's jaw bones following implant insertion and a photoelastic study of implants and the jaw bones. *J Osaka Dent Univ* 7:31-42.

Koeck B, Sander G (1978). Über die elastische Deformation der Unterkieferspange. *Dtsch Zahnärztl Z* 33:254-261.

Korioth TWP (1992). Finite element modelling of human mandibular biomechanics (thesis). Vancouver (BC): The University of British Columbia.

Korioth TWP, Romilly DP, Hannam AG (1992). Three-dimensional finite element stress analysis of the dentate human mandible. *Am J Phys Anthropol* 88:69-96.

Lees S, Rollins FR, Jr (1972). Anisotropy in hard dental tissues. *J Biomechan* 5:557-566.

Mandel U, Dalgaard P, Viidik A (1986). A biomechanical study of the human periodontal ligament. *J Biomechan* 19:637-645.

Marx H (1966). Untersuchungen der funktionsbedingten elastischen Deformierung der menschlichen Mandibula. *Dtsch Zahnärztl Z* 21:937-938.

McDowell JA, Regli CP (1961). A quantitative analysis of the decrease in width of the mandibular arch during forced movements of the mandible. *J Dent Res* 40:1183-1185.

Mühlemann HR, Zander H (1954). The mechanism of tooth mobility. *J Periodont* 25:128-135.

Omar R, Wise MD (1981). Mandibular flexure associated with muscle force applied in the retruded axis position. *J Oral Rehabil* 8:209-221.

Osborn JW (1961). An investigation into the interdental forces occurring between the teeth of the same arch during clenching the jaws. *Arch Oral Biol* 5:202-211.

Osborne J, Tomlin HR (1964). Medial convergence of the mandible. *Br Dent J* 117:112-114.

Picton DCA (1962). Distortion of the jaws during biting. *Arch Oral Biol* 7:573-580.

Pruim GJ, de Jongh HJ, ten Bosch JJ (1980). Forces acting on the mandible during bilateral static bite at different bite force levels. *J Biomechan* 13:755-763.

Ralph WJ (1982). Tensile behaviour of the periodontal ligament. *J*

Periodont Res 17:423-426.

Regli CP, Kelly EK (1967). The phenomenon of decreased mandibular arch width in opening movements. *J Prosthet Dent* 17:49-53.

Southard TE, Southard KA, Tolley EA (1990). Variation of approximal tooth contact tightness with postural change. *J Dent Res* 69:1776-1779.

Weijs WA, de Jongh HJ (1977). Strain in mandibular alveolar bone during mastication in the rabbit. *Arch Oral Biol* 22:667-675.

Weijs WA, Hillen B (1984). Relationship between the physiological cross-section of the human jaw muscles and their cross-sectional area in computer tomographs. *Acta Anat* 118:129-138.

Widera GEO, Tesk JA, Privitzer E (1976). Interaction effects among cortical bone, cancellous bone and periodontal membrane of natural teeth and implants. *J Biomed Mater Res Symp* 7:613-623.

Wong M, Carter DR (1988). Mechanical stress and morphogenetic endochondral ossification of the sternum. *J Bone Joint Surg* 70(A):992-1000.